IEEE Photonics Journal
An IEEE Photonics Society Publication

Open Access

Impulse Response Modeling of Underwater Optical Scattering Channels for Wireless Communication

Volume 12, Number 4, August 2020

Rubén Boluda-Ruiz
Pedro Rico-Pinazo
Beatriz Castillo-Vázquez
Antonio García-Zambrana
Khalid Qaraqe

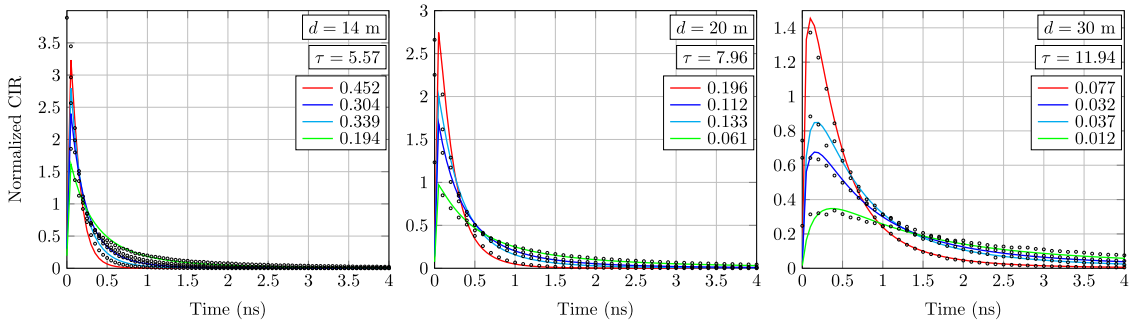

DOI: 10.1109/JPHOT.2020.3012302

Impulse Response Modeling of Underwater Optical Scattering Channels for Wireless Communication

Rubén Boluda-Ruiz,[1] **Pedro Rico-Pinazo**,[1]
Beatriz Castillo-Vázquez,[1] **Antonio García-Zambrana**,[1]
and Khalid Qaraqe [2]

[1]Andalucía Tech, Department of Communications Engineering, Campus de Teatinos, University of Málaga, Málaga 29071, Spain
[2]Department of Electrical, and Computer Engineering, Texas A&M University at Qatar, Doha 23874, Qatar

DOI:10.1109/JPHOT.2020.3012302

Manuscript received May 15, 2020; revised July 21, 2020; accepted July 24, 2020. Date of publication July 28, 2020; date of current version August 10, 2020. This work was supported in part by the Programa Operativo I+D+i FEDER Andalucía 2014-2020 under Grant UMA18-FEDERJA-099 and in part by the Spanish MICINN Project under Grant PID2019-107792GB-I00. This article was presented in part at the 2019 IEEE Global Communications Conference (GLOBECOM) in Waikoloa, HI, USA, December 2019 [1]. Corresponding author: Rubén Boluda-Ruiz (e-mail: rbr@ic.uma.es).

Abstract: Despite the fact that underwater optical wireless communication (UOWC) systems are able to provide high-data rate links with high security, the performance of these systems presents several limitations related to the maximum achievable distance due to attenuation, and scattering effects. Hence, quantifying the signal attenuation, and the time-dispersion produced by such effects represents a crucial work in channel modeling. Motivated by this, we present, for the first time, a novel, and unified impulse response modeling of underwater optical scattering channels based on the superposition of one impulsive component, and one dispersive component with two degrees of freedom. We provide analytical results for channel path loss, and channel impulse response (CIR) which are validated through Monte-Carlo simulations based on photon-tracing for clear ocean, coastal, and harbor waters. In order to provide a physical insight, the developed CIR is used to compute the root-mean-square (RMS) delay spread as a function of distance, and type of water, as well as to analyze in greater detail the impact of inter-symbol interference (ISI) on the data rate. These outcomes can be used for high-speed systems design, and optimization.

Index Terms: Underwater optical wireless communication (UOWC), Channel impulse response (CIR), Henyey-Greenstein model, Monte-Carlo simulation.

1. Introduction

1.1 Motivation

Given the huge interest in everything related to the marine environment, which is justified by a large number of environmental and resource generation reasons, the challenge of extending the telecommunication networks to the underwater environment is now a reality. Moreover, in recent years, with the threat of increasingly evident global climate change and the foreseeable

depletion of many resources, there is a strong and increasing interest in ocean exploration systems. In fact, up to 95% of the ocean is still unexplored or insufficiently exploited [2]. Within this context, promoting research and development on underwater optical wireless communication (UOWC) systems has become even more important. It is clear that there is an urgent need to explore the enormous potential of these systems compared to conventional acoustic systems, with a very limited inherent transmission rate, and compared to radio-frequency (RF) systems in terms of their range, just a few centimeters at practical frequency values. UOWC systems can be used in a great deal of potential applications related to underwater observation or even rescue scenarios such as links between autonomous underwater vehicles (AUV), telemetry, links between divers, real-time video transmission, among others [3]. In these scenarios, the use of UOWC systems in the blue-green band (450–570 nm) is a very interesting and attractive solution for underwater communications due to their large bandwidth on the order of MHz at moderate distances (10–100 m) [4], providing high data rates, low latency and low power consumption [5]–[7]. However, despite the advantages that UOWC systems present in dealing with the aforementioned societal challenges, such systems have a series of drawbacks that must be taken into account in order to analyze in greater detail the limit of achievable performance [8]. It is evident that the main limiting agent of such communication systems is the strong attenuation produced by the processes of absorption and scattering, which can be rigorously described by the inherent optical characteristics of the water [9]. While the absorption process, which is an irreversible process due to the interaction of the light beam with water molecules and other particles, is mitigated through the use of wavelengths in the blue-green band, the scattering process presents a relevant impact by changing the direction of the transmitted photons. This leads to a significant temporal dispersion that results in inter-symbol interference (ISI) by causing miscommunication in the receiver's decision system. Undoubtedly, characterizing accurately the degree of scattering of UOWC systems through the channel impulse response (CIR) represents an important milestone in channel modeling.

1.2 Related Work

CIR modeling of UOWC has been carried out in the last few years [10]–[15]. All these reported works have a common denominator: all of them fail to provide a complete model for computing both channel path loss and channel impulse response. In relation to the time-dispersion produced by absorption and scattering, some research works have been reported [10]–[13]. Based on the impulse response in clouds, the double function Gamma (DGF) is proposed in [10] to model the CIR by using four degrees of freedom. It should be noted that, although the results are accurate thanks mainly to the use of four degrees of freedom, the physical characteristics of clouds are substantially different from those for the water. In [13], also using four degrees of freedom, a function based on a combination of exponential and arbitrary power function (CEAPF) is proposed. None of these reported works was capable of providing evidences of the physical relation between the phenomena of absorption and scattering and the proposed mathematical model. In addition, all these reported models are only valid for turbid environments. On the other hand, the intensity attenuation associated with the UOWC channel has been also reported in [14], [15]. In [14], a closed-form expression for channel path loss is presented for different types of water, which is only valid for semi-collimated sources. The developed expression is also used to determine the maximum achievable UOWC link. In [15], four different Monte-Carlo methods are presented for multiple scattering channels in optical wireless communications, where analytical results for computing channel path loss and channel impulse response are not provided. Motivated by the above, we focus on the CIR modeling as the main channel characteristic in strongly scattering media.

TABLE 1
Extinction Coefficients for Different Types of Water

Water type	$a[m^{-1}]$	$b[m^{-1}]$	$c[m^{-1}]$
Clear ocean	0.114	0.037	0.151
Coastal	0.179	0.219	0.398
Harbor	0.366	1.824	2.190

1.3 Contributions and Novelties

The main contributions and novelties of this paper are summarized as follows:

- We aim to model the CIR of UOWC systems with high precision by using a new approach based on the albedo definition. We analyze the CIR of UOWC systems by taking into account channel path loss in different scattering conditions such as clear ocean, coastal and harbor waters, as well as for different transmitter sources such as laser diode (LD) and light emitting diode (LED), and different values of the receiver field-of-view (FOV).
- The developed expression, which is even expressed as a function of distance, is obtained as a superposition of one impulsive component that is associated with the line-of-sight (LOS), and one dispersive component that represents those transmitted photons that are scattered multiple times. The proposed CIR modeling is consistent with all types of water due to the fact that when the impulsive component becomes important, the dispersive component becomes less significant, and vice-versa. This result is of special importance since we can compute the CIR for all types of water, which makes this model be much more versatile.
- By exploiting the proposed CIR, we also aim to review the temporal dispersion of the underwater optical channel from the root-mean-square (RMS) delay spread point of view, resulting in being a very important design parameter to get reliable UOWC links.
- Unlike the prior reported works [10]–[15], this work represents an unprecedented research work due to the lack of a generic CIR analysis. We present a new and unified CIR model based on the mixture of two Gamma functions that fits much better with photon-tracing-based Monte-Carlo simulations, and that takes into account channel path loss. Moreover, this analytical model is valid for all types of water as a consequence of modeling the CIR as a superposition of one impulsive component and one dispersive component, which is much more mathematically tractable and computationally efficient with only two degrees of freedom.

1.4 Organization

The remainder of this paper is arranged as follows. Firstly, in Section 2, a general underwater optical channel that is affected by absorption and scattering is described. In Section 3, a careful analysis of the CIR modeling of UOWC systems is presented, paying special attention to the strength of the scattering effect. Some practical UOWC examples are provided in Section 4 for different scattering conditions. Finally, the paper is concluded in Section 5.

2. Characterization of the Underwater Optical Channel

As commented above, the underwater optical channel is highly vulnerable to the effects of absorption (a) and scattering (b), which are characterized through the extinction coefficient as $c(\lambda) = a(\lambda) + b(\lambda)$ [m^{-1}], with λ being wavelength. Note that the values of $a(\lambda)$ and $b(\lambda)$ depend on inherent optical properties of the water, which depend on the wavelength and the kind of particulate and dissolved matter in the ocean. Here, the values of $a(\lambda)$ and $b(\lambda)$ for clear ocean, coastal and harbor waters are summarized in Table 1 when considering a wavelength of 532 nm [9], [16]. Hereinafter, $a(\lambda)$, $b(\lambda)$, and $c(\lambda)$ are denoted by a, b, and c, respectively.

In order to analytically predict the CIR and provide a unified model, we use a Monte-Carlo simulations method to numerically compute the effects of absorption and scattering on underwater light

beam propagation by sending a large amount of photons (on the order of 10^{11}) and simulating their interaction with the medium, as normally used in the current literature [17]. During the simulation process, the photon weight is modified according to the albedo definition such that the new weight is multiplied by b/c, and the photon direction is also modified in each interaction with the medium. This new direction is obtained from the scattering function that determines the new propagation direction. The angular distribution of scattering in water used in the simulation process is the Henyey-Greenstein (HG) phase function [18]. Despite the fact that there are different techniques for UOWC channel modeling in the existing literature, Monte-Carlo method presents inherent advantages that makes it optimum for modeling such a dispersive communication channel [19]. Moreover, Monte-Carlo method based on photon tracing has been also used to model the CIR of non-LOS ultraviolet scattering communication channels [20].

As with the atmospheric optical channel [21], [22] (and references therein), the underwater optical channel also exhibits random fluctuations in the refractive index, i.e. oceanic turbulence, mainly due to fluctuations in physical parameters such as salinity and temperature. Although its impact can be considered neglected in deep waters [23], it must be highlighted that we neglect the effect of oceanic turbulence in this paper to fully focus on the effects of absorption and scattering.

3. Channel Impulse Response (CIR) Modeling

In this section, our purpose is to find a prototypical channel impulse response from Monte-Carlo simulations based on photon tracing.

3.1 Previous Work

For convenience and, as a reference, we reproduce briefly some of the reported models mentioned in Section 1. As commented, the authors in [10, Eq. (10)] proposed the DGF to model the impulse response that is based on the properties of clouds. In this way, the CIR expression as a function of time, t, is given by

$$h_1(t) = C_1 \cdot t \cdot e^{-C_2 t} + C_3 \cdot t \cdot e^{-C_4 t}, \tag{1}$$

where C_1, C_2, C_3, and C_4 are the four parameters to be found through Monte-Carlo simulations. At the same time, a new function model based on CEAPF was recently proposed in [13, Eq. (13)] as follows

$$h_2(t) = C_1 \frac{t^{\alpha}}{(t + C_2)^{\beta}} e^{-\alpha v t}, \tag{2}$$

where $C_1 > 0$, $C_2 > 0$, $\alpha > -1$, and $\beta > 0$ are the four parameters to be found through Monte-Carlo simulations, and v is the speed of light in water. Note that none of these CIR models are valid for water types in which the effect of scattering is not as dominant as in turbid environments. In addition, these models do not take into account channel path loss either.

3.2 Proposed CIR Analysis

Let us model the CIR, h, as a stochastic process from the albedo definition as $h = b/c$. In this model, both parameters follow a Gamma distribution as

$$f_b(x) = \frac{\alpha_1^{\beta_1}}{\Gamma(\beta_1)} \exp(-\alpha_1 \cdot x) \cdot x^{\beta_1 - 1}, \tag{3a}$$

$$f_c(y) = \frac{\alpha_2^{\beta_2}}{\Gamma(\beta_2)} \exp(-\alpha_2 \cdot y) \cdot y^{\beta_2 - 1}, \tag{3b}$$

where α_1 and α_2 are the shape parameters, β_1 and β_2 are the scale parameters, and $\Gamma(\cdot)$ is the Gamma function. We obtain the CIR by solving the below conditional integral by doing $b = h \cdot c$ as

follows

$$h_{\mathrm{BP}}(t) = \int_0^\infty f_b(t|y) f_c(y) dy. \tag{4}$$

Now, by substituting Eq. (3) into Eq. (4), we obtain $h_{\mathrm{BP}}(t)$ as

$$h_{\mathrm{BP}}(t) = \frac{\alpha_1^{\beta_1}\alpha_2^{\beta_2}}{\Gamma(\beta_1)\Gamma(\beta_2)} t^{\beta_1-1} \int_0^\infty \frac{\exp[-(\alpha_1 t + \alpha_2)y]}{y^{-\beta_1-\beta_2+2}} dy. \tag{5}$$

If we particularize for $\alpha_1 = \alpha_2$, the above integral can be computed with the help of [24, Eq. (3.326.2)], obtaining the Beta Prime (BP) distribution [25] as follows

$$h_{\mathrm{BP}}(t) = \frac{\Gamma(\beta_1+\beta_2)}{\Gamma(\beta_1)\Gamma(\beta_2)} \cdot \frac{t^{\beta_1-1}}{(1+t)^{\beta_1+\beta_2}}, \quad t > 0, \tag{6}$$

where $\beta_1 > 0$, and $\beta_2 > 0$ are the parameters to be solved. These parameters can be found by using nonlinear least square criterion as follows

$$(\beta_1, \beta_2) = \arg\min \left(\int [h_{\mathrm{BP}}(t) - h_{\mathrm{MC}}(t)]^2 dt \right), \tag{7}$$

where $h_{\mathrm{BP}}(t)$ is obtained via Eq. (6), and $h_{\mathrm{MC}}(t)$ is evaluated via Monte-Carlo simulations. The above equation is evaluated via curve fitting approach using mathematical software packages such as Wolfram Mathematica. Note that we have selected the Gamma distribution to model the dispersive component of the CIR due to the fact that this distribution has demonstrated to be an excellent approximation for many propagation problems [26].

Keeping in mind that our main goal is to present a CIR modeling that does not only fit well with strongly scattering media, but also with media where the scattering effect is not as dominant, we propose to model the CIR as a superposition of one impulsive component and one dispersive component. Note that this approach has never been used in the current literature to model the CIR of UOWC systems. On the one hand, when scattering is not dominant, the CIR can be modeled as a delta Dirac function, i.e., an impulsive component with its corresponding ballistic delay. This is due to the fact that the transmitted photons are not scattered multiple times and, hence, they are capable of reaching the photodetector through the LOS. This is also usually referred to as a flat channel so that the transmitted signal will experience negligible ISI. On the other hand, the dispersive component is modeled as in Eq. (6). Therefore, we propose, for the first time, a generalized closed-form expression to model the CIR in UOWC systems as follows

$$h_0(t) = (1-k) \cdot \delta(t) + k \cdot h_{\mathrm{BP}}(t), \tag{8}$$

where $k \in [0, 1]$ is the parameter that determines how important one of the components is with respect to the other one. The parameter k is computed from the first sample of Monte-Carlo simulation and represents all those photons that arrive through the non-LOS. Finally, the expression in Eq. (8) can be rewritten in a more compact-form as follows

$$h(t) = H(0) \cdot h_0(t) \cdot u(t), \tag{9}$$

where $u(t)$ is the step function, $h_0(t)$ is the normalized CIR with $\int_0^\infty h_0(t)dt = 1$, and $H(0)$ is channel gain or path loss given by

$$H(0) = \int_0^\infty h(t) dt. \tag{10}$$

As it is well-known, channel path loss is computed as a function of link distance according to the Beer Lambert's law. However, this law only computes the path loss associated with the LOS and, hence, underestimating the dispersive component that allows to recollect more photons, specially those that are reflected multiple times until reaching the receiver. Thus, we present a modified version of the Beer Lambert's law to include the effect of scattering as follows

$$\mathrm{H}(0)[dB] \simeq 10 \log_{10}(\mathrm{GL}(d) \cdot e^{-F_c \cdot c(\lambda) \cdot d}), \tag{11}$$

where GL stands for geometric loss, and F_c is a correcting factor that is given by

$$F_c = \ln\left(\frac{\mathrm{GL}(d)}{\int_0^\infty h_{\mathrm{MC}}(t,d)dt}\right) \Big/ c(\lambda)\cdot d, \tag{12}$$

where $h_{\mathrm{MC}}(t,d)$ is the simulated CIR at link distance d, and the integral of $h_{\mathrm{MC}}(t,d)$ is the area of such a CIR. Regarding GL, when assuming an LD with a Gaussian beam profile, GL is given by [27] as follows

$$\mathrm{GL}_{\mathrm{LD}}(d) = \frac{A_{\mathrm{PD}}}{\pi(d\cdot\tan\theta_{div})^2} \simeq \frac{D^2}{4(d\cdot\theta_{div})^2}, \tag{13}$$

where A_{PD} is the area of a circular receiver aperture, D is the receiver aperture diameter, and θ_{div} is the divergence angle. When assuming an LED with Lambertian emission, GL is given by

$$\mathrm{GL}_{\mathrm{LED}}(d) = \frac{A_{\mathrm{PD}}(m+1)}{2\pi d^2}\cos^m\phi = \frac{D^2(m+1)}{8d^2}\cos^m\phi, \tag{14}$$

where $\cos\phi$ is the angle of irradiance, and $m = -1/\log_2(\theta_0/2)$ is the order of the Lambertian emission with θ_0 the divergence angle.

3.3 CIR Modeling as a Function of Distance

In an attempt to model analytically the parameters involved in the proposed prototypical CIR, we now present a set of three closed-form expressions to compute the parameters k, β_1 and β_2 as a function of distance, which are solved from Monte-Carlo simulations. We have observed from such simulations that both channel path loss and channel impulse response are highly distance-dependent, confirming that the distance of UOWC systems is a key feature in the performance of UOWC systems. Hence, this set of expressions is of great relevance to analyze, for instance, the RMS delay spread as we will see in the next section, as well as for channel modeling and performance evaluation purposes. Firstly, we present the closed-form expression of $k(d)$ which allows us to study in greater detail when one of the components is more dominant than the other one, i.e., how significant the effect of scattering is. According to our Monte-Carlo simulations, the parameter k presents an exponential behavior, and it can be expressed as

$$k(d) \simeq k_a - k_b e^{-k_c\cdot d}, \tag{15}$$

where k_a, k_b, and k_c are the parameters to be solved from the Monte-Carlo simulation. Secondly, we present the parameter β_1 as a function of distance. This parameter has a double behavior that depends on the type of water and the UOWC link distance: β_1 presents a decaying exponential distance dependence for attenuation lengths, $\tau = d\cdot c$, smaller than 10 approximately, whereas for attenuation lengths larger than 10, β_1 presents a growing quadratic distance dependence. In fact, it was demonstrated in [17], [28], [29] that for attenuation lengths larger than 10, the effect of scattering becomes significant, and it predominates for larger than 15. As we will see in the next section, this effect translates into a change of trend in β_1 as a function of distance. Thus, the parameter β_1 can be modeled as

$$\beta_1(d) \simeq \begin{cases} \beta_{1a} + \beta_{1b}e^{-\beta_{1c}\cdot d}, & d\cdot c < 10 \\ \beta_{1a}\cdot d^2 + \beta_{1b}\cdot d + \beta_{1c}, & d\cdot c \geq 10. \end{cases} \tag{16}$$

where β_{1a}, β_{1b}, and β_{1c} are the parameters to be solved from the Monte-Carlo simulation. Thirdly, we present the parameter β_2 as a function of distance as follows

$$\beta_2(d) \simeq \beta_{2a} + \beta_{2b}e^{-\beta_{2c}\cdot d}, \tag{17}$$

where β_{2a}, β_{2b}, and β_{2c} are the parameters to be solved from the Monte-Carlo simulation. In the next section, we will check how these parameters behave as a function of distance for different UOWC scenarios in different scattering conditions.

TABLE 2
UOWC System Parameters

Parameter	Symbol	Value
Wavelength	λ	532 nm
UOWC link distance	d	{5,12,14,20,30,35,50} m
Water refractive index	n	1.3
LD divergence angle at $1/e$	θ_{div}	10°
LD beam waist radius	w_z	10 mm
LED divergence angle (full-angle)	θ_0	80°
Receiver aperture diameter	D	50 cm
Receiver FOV	FOV	$\{20^{\circ}, 180^{\circ}\}$
Number of transmitted photons	N_T	10^{11}
Photon weight threshold	W_{th}	10^{-6}

4. Numerical Results and Discussion

In this section, we compute channel impulse response of UOWC systems both numerically via Monte-Carlo simulation and analytically via Eq. (8) for different types of water (clear ocean, coastal and harbor), as summarized in Table 1. For simulation purposes, the UOWC system parameters assumed in this paper, which are used in real UOWC scenarios, are summarized in Table 2.

4.1 Results of Channel Impulse Response

In Fig. 1, we can see how the proposed CIR matches very well with Monte-Carlo simulations regardless of water type, source type, link distance and FOV values. This prototypical CIR is able to fit with a great variety of water types such as clear ocean, coastal and harbor by using only one mathematical expression. More importantly, this accuracy is achieved using only two degrees of freedom (β_1 and β_2) to model the dispersive component in comparison with [10], [13] that use four degrees of freedom each. For the sake of intelligibility, there is a small legend in each subfigure to specify the value of the weight of the impulsive component, i.e. $(1 - k)$, for each scenario considered. Note that this value basically decreases as the link distance and/or turbidity of water increase. For that reason, the peak of the CIR associated with the dispersive component is less significant in clear ocean water than in coastal and harbor waters. It is also seen that the peak of the CIR is shown up slightly later in some scenarios such as 20 m UOWC link in harbor water. The reason behind this is that too fewer photons are able to reach the receiver through the LOS and, hence, they are delayed in arriving at. We can also see how the CIR spreads due to both the increase in link distance and the increase in turbidity level of the type of water. This is deeply related to the attenuation length, τ. At the same time, there is a notable difference when using an LD instead of an LED due to the high directivity of an LD that is reflected in higher peaks of the CIR.

In Fig. 2, we plot the CIR parameters $k(d)$, $\beta_1(d)$ and $\beta_2(d)$ as a function of distance for different water types, source type, and different values of FOV. In the light of this figure, we can conclude that the analytical results obtained via Eqs. (15), (16) and (17) also match very well with Monte-Carlo simulations. Having the CIR expressed not only as a function of time, but also as a function of distance represents a key milestone in CIR modeling for reliable UOWC systems design. Theses expressions will be used to study key indicators such as RMS delay spread as well as the range of distances at which the underwater optical channel behaves as an impulsive one or as a dispersive one.

With regard to the parameter $k(d)$, it is observed from Fig. 2(a) that as the attenuation length increases, the impulsive component becomes less important, i.e., the CIR is highly distance-dependent, limiting the maximum achievable distance. In other words, the weight of the dispersive component, i.e. $k(d)$, presents the same trend as the attenuation length. Both of them increase when the UOWC link distance increases. However, the parameter $k(d)$ increases up to 1, which would mean that the underwater channel is purely of non-impulsive nature. From Fig. 2(c), it

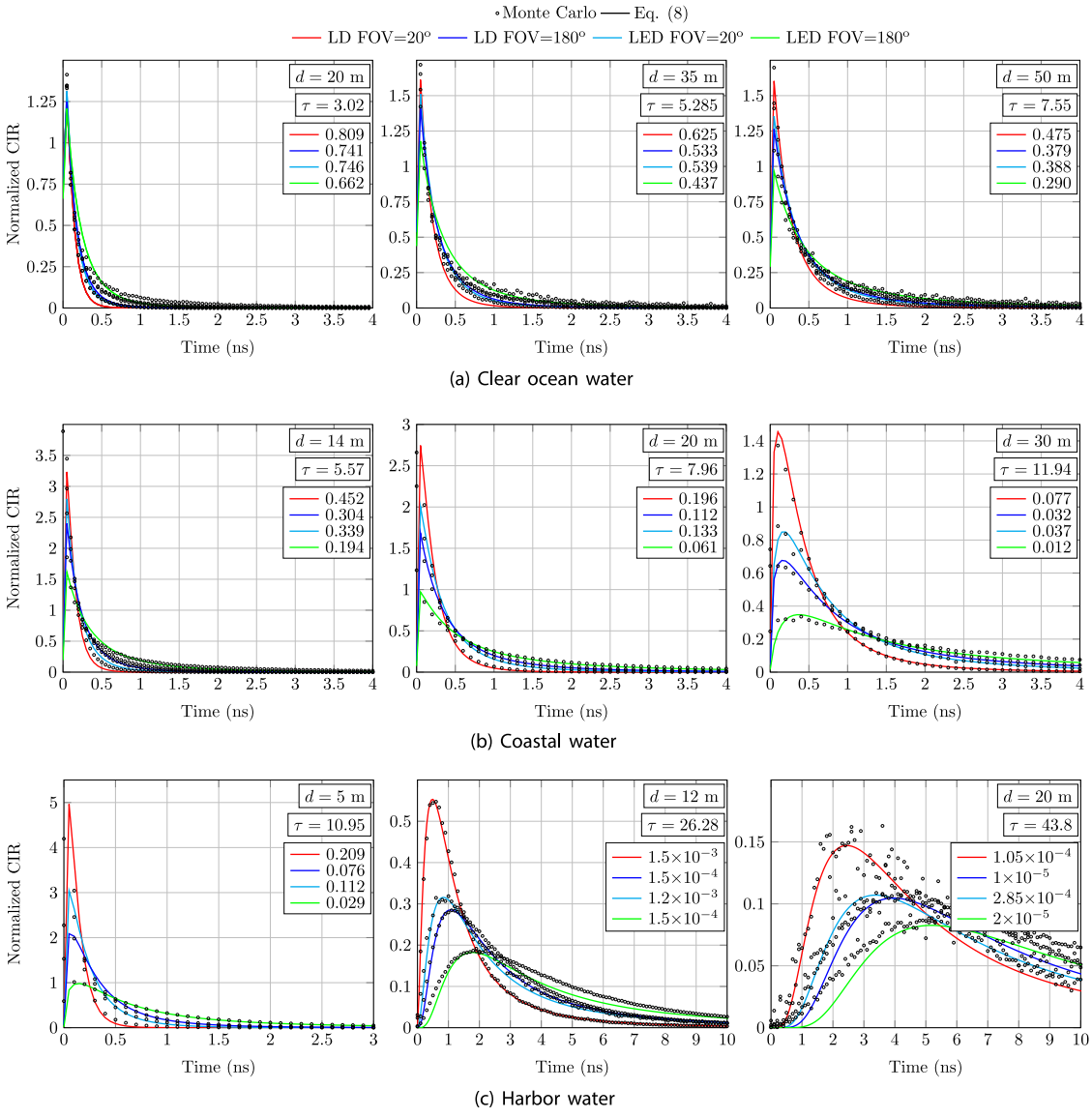

Fig. 1. Normalized CIR, $h_0(t)$, for (a) clear ocean, (b) coastal, and (c) harbor waters when different distances of $d = \{5, 12, 14, 20, 30, 35, 50\}$ m, different transmitter sources (LD and LED) and different values of FOV $= \{20^\circ, 180^\circ\}$ are considered. Note that, for the sake of clarity, Monte-Carlo simulation results in some subfigures are depicted by considering a sampling period of 0.1 ns. However, the Monte-Carlo simulation tool developed for this paper uses a sampling period of 0.05 ns. In order to highlight the value that the normalized CIR takes at the origin, i.e., the weight of the impulsive component, which is computed as $h_0(t)$ at $t = 0$, we have added a small legend in each subfigure to specify this value for each scenario.

can be observed a certain relation between $k(d)$ and $\beta_2(d)$. According to our simulations, $\beta_2(d)$ presents a decaying exponential distance dependence, showing a similar trend to the energy of the impulsive component. On the contrary, $\beta_1(d)$ is much more sophisticated than $\beta_2(d)$. From a mathematical point of view, $\beta_1(d)$ presents a double behavior, as we can see in Fig. 2(b). For very short distances, i.e. when the effect of scattering is not so significant, $\beta_1(d)$ presents a decaying exponential distance dependence. This phenomenon is only observed in clear ocean water, and it is related to the attenuation length, τ. Due to the relatively small values of the attenuation length in

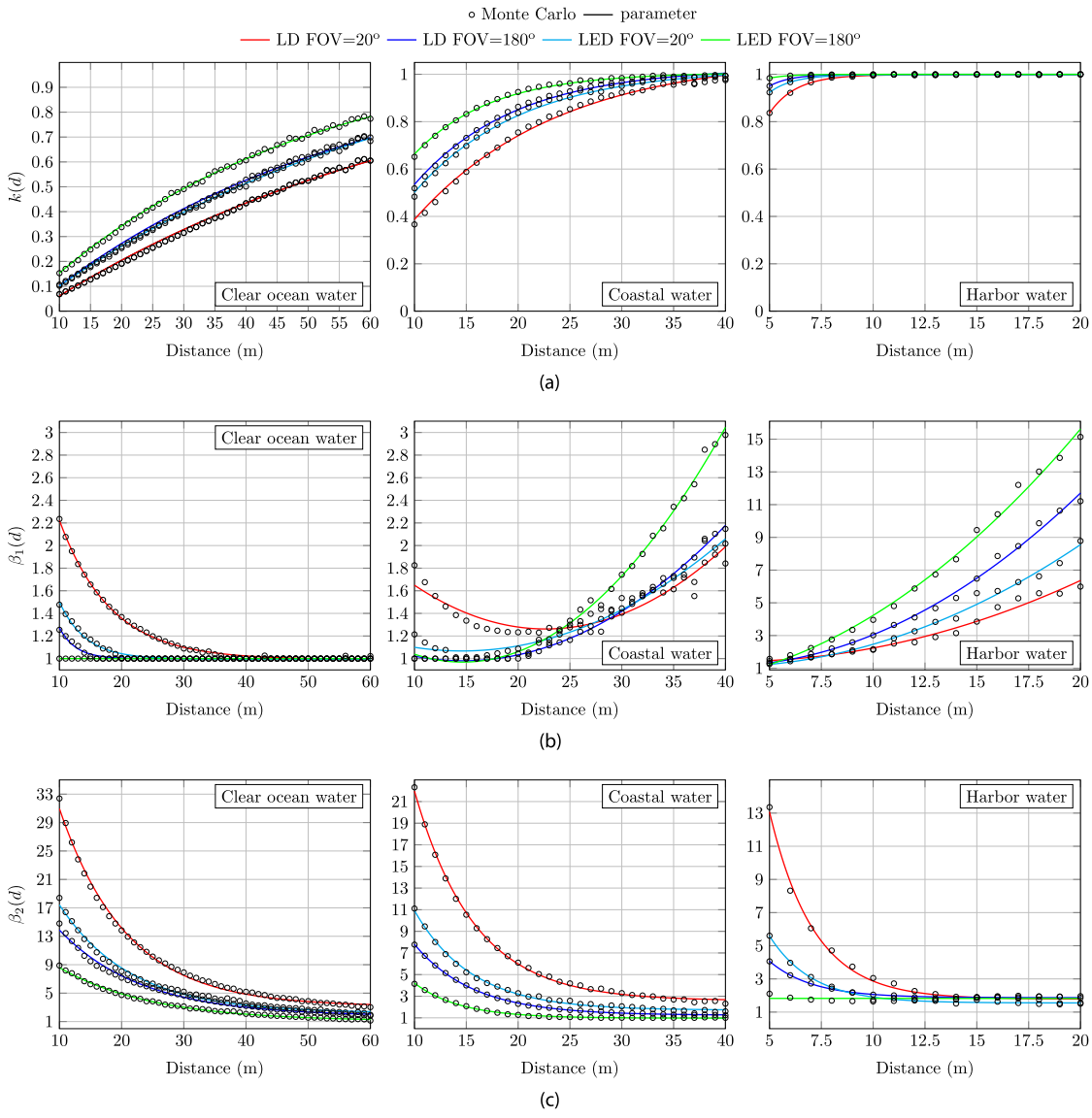

Fig. 2. Parameters (a) $k(d)$, (b) $\beta_1(d)$, and (c) $\beta_2(d)$ as a function of distance for clear ocean, coastal and harbor waters when a receiver aperture diameter of $D = 50$ cm and different transmitter sources are considered for different values of the receiver FOV.

coastal and harbor waters, a decaying exponential distance dependence is not observed for $\beta_1(d)$ when very short distances are considered. By other hand, it is found out that there is a turning value of the attenuation length that results in the scattering effect to become really significant. This leads to a change of trend in $\beta_1(d)$, making this parameter grow in distance. When τ is above 10, approximately for 25 m in coastal water and for 5 m in harbor water, $\beta_1(d)$ starts to increase by following a quadratic distance dependence. However, this effect does not seem to be observed in clear ocean water due to the fact that the scattering effect is not very significant in this kind of water, making $\beta_1(d)$ tend to one as distance increases. The turning value of the attenuation length that makes a slight change of trend in clear ocean water occurs above 80 m approximately. These results were omitted since this distance may be unpractical for potential UOWC applications and, hence, the UOWC system may not provide a good performance. Hence, as the water gets turbid,

$\beta_1(d)$ tends to a growing quadratic distance dependence because of the impact of scattering at moderate distances. We conclude that this change of trend can be perfectly attributable to an increase in the severity of scattering.

Next, with the goal of quantifying when one of the components of the CIR is dominant with respect to the other one, we can find the range of distances mentioned above. To do that, we use the relation between the weight of the impulsive component $(1 - k(d))$ and the weight of the dispersive component $(k(d))$. Let us assume that the underwater channel behaves as impulsive when this relation is equal to $\sqrt{2}$ following the same criterion of 3-dB bandwith. At the same time, when this relation is equal to $1/\sqrt{2}$, the underwater channel behaves as dispersive. Hence, the range of distances that determines this interesting behavior is derived from $(1 - k(d))/k(d)$ as follows

$$d_\delta = \frac{1}{k_c} \ln\left(k_b/(k_a - 0.414)\right), \tag{18a}$$

$$d_{\text{BP}} = \frac{1}{k_c} \ln\left(k_b/(k_a - 0.585)\right). \tag{18b}$$

The above equations indicate that when the UOWC link distance d is below d_δ, i.e. $d \leq d_\delta$, the underwater channel is clearly of impulsive nature, and when d is above d_{BP}, i.e. $d \geq d_{\text{BP}}$, the underwater channel is of non-impulsive nature. When the distance is between d_δ and d_{BP}, i.e. $d_\delta < d < d_{\text{BP}}$, we cannot say that one of the component is dominant with respect to the other one since both of them present an impact on the CIR in terms of the signal attenuation and temporal dispersion.

For the sake of clarity, we will give some practical values of such distances for clear ocean water since this scenario allows to achieve longer communication distances. Thus, when an LD at the transmitter-side and a value of the receiver FOV of 180° are used, the range of distances is equal to $(d_\delta, d_{\text{BP}}) = (30.35, 46.24)$ m, y when an LED at the transmitter-side and a value of the receiver FOV of 180° are used, the range of distances is equal to $(d_\delta, d_{\text{BP}}) = (24.55, 37.8)$ m. Taking into account the above values, we can observe that for UOWC link distances in clear ocean water below 30 m and 24 m, we can consider the underwater channel as an impulsive one when an LD and an LED are used, respectively. On the contrary, for UOWC link distances above 46 m and 37 m, we can consider the underwater channel as a non-impulsive one when an LD and an LED are used, respectively. The thing is totally different when studying turbid environments such as coastal and harbor waters since the underwater channel behaves as a non-impulse or dispersive one for UOWC link distances above ∼10 m and ∼5 m, respectively, regardless of the source type and the receiver FOV.

To quantify the achieved accuracy of the CIR modeling proposed in this paper, we have evaluated the coefficient of determination R-square (R^2) for all scenarios considered in Fig. 1. As highlighted in red in Table 3, the predicted CIR achieves a value of R^2 always above 0.97 regardless of the type of water and the type of transmitter source. In general, this accuracy is well above the values of R^2 achieved by the different models proposed in the current literature [10], [13]. It should be noted that the approach proposed in this article is far superior in view of the results presented, achieving a precision that in the worst case is equal to those already reported in the literature and using less degrees of freedom. Unlike the reported models, which are only valid for turbid environments, this model is valid for three types of water such as clear ocean, coastal and harbor waters. Particularly, the proposed model is able to get a remarkable superiority in clear ocean water. This UOWC scenario has not been considered yet in the existing literature due to the difficulty in providing with a complete CIR modeling. Additionally, we have also computed the coefficient of determination R^2 for the CIR parameters $k(d)$, $\beta_1(d)$ and $\beta_2(d)$ for all the considered scenarios, obtaining always a value above 0.95.

TABLE 3
Values of the Coefficient of Determination R-Square (R^2) for Different Types of Water

Clear ocean water				Coastal water				Harbor water			
d (m)	Eq. (1)	Eq. (2)	Eq. (8)	d (m)	Eq. (1)	Eq. (2)	Eq. (6)	d (m)	Eq. (1)	Eq. (2)	Eq. (8)
LD-FOV $= 20°$											
20	0.010	0.010	0.986	14	0.022	0.022	0.991	5	0.301	0.301	0.996
35	0.038	0.038	0.991	20	0.277	0.277	0.996	12	0.996	0.999	0.999
50	0.084	0.084	0.994	30	0.731	0.732	0.997	20	0.981	0.989	0.982
LD-FOV $= 180°$											
20	0.013	0.013	0.986	14	0.118	0.118	0.992	5	0.757	0.758	0.999
35	0. 047	0.047	0.985	20	0.452	0.454	0.998	12	0.996	0.999	0.996
50	0.103	0.103	0.988	30	0.866	0.875	0.996	20	0.981	0.999	0.990
LED-FOV $= 20°$											
20	0.014	0.014	0.988	14	0.102	0.102	0.994	5	0.612	0.612	0.998
35	0.050	0.050	0.991	20	0.423	0.424	0.998	12	0.998	0.998	0.999
50	0.109	0.109	0.993	30	0.834	0.840	0.996	20	0.970	0.977	0.970
LED-FOV $= 180°$											
20	0.019	0.019	0.972	14	0.249	0.249	0.984	5	0.921	0.925	0.999
35	0.062	0.062	0.974	20	0.631	0.641	0.996	12	0.997	0.999	0.999
50	0.135	0.137	0.981	30	0.935	0.947	0.984	20	0.984	0.998	0.996

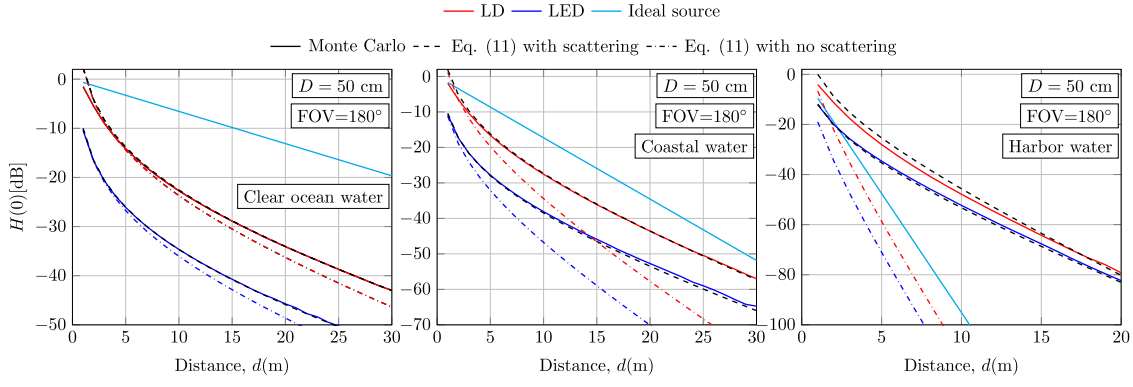

Fig. 3. Channel path loss as a function of distance for clear ocean, coastal and harbor waters when a receiver FOV $= 180°$ and a receiver aperture diameter of $D = 50$ cm are considered for different transmitter sources.

4.2 Results of Channel Path Loss

In Fig. 3, channel path loss is represented as a function of the UOWC link distance when different types of water are considered for a receiver FOV value of 180°, as normally used in practice, as well as for different transmitter sources such as LD (in red color) and LED (in blue color). The results obtained via Monte-Carlo simulations are depicted with solid curves, and the analytical results obtained via Eq. (11) are depicted with dashed lines. As a reference, the analytical results obtained via Eq. (11) for an ideal source ($GL = 1$) with no scattering ($F_c = 1$) are also included in cyan color. As we can observe from this figure, the expression developed in this paper allows us to evaluate channel path loss with high precision. As expected, channel path loss decreases as the link distance increases regardless of the rest of major system parameters. The results obtained for harbor water are really striking, reaching a value of approximately 80 dB for an UOWC link distance of 20 m. These losses clearly limit the maximum achievable distance not only in this type of water, but also in the other scenarios (clear ocean and coastal waters) considered here, requiring more

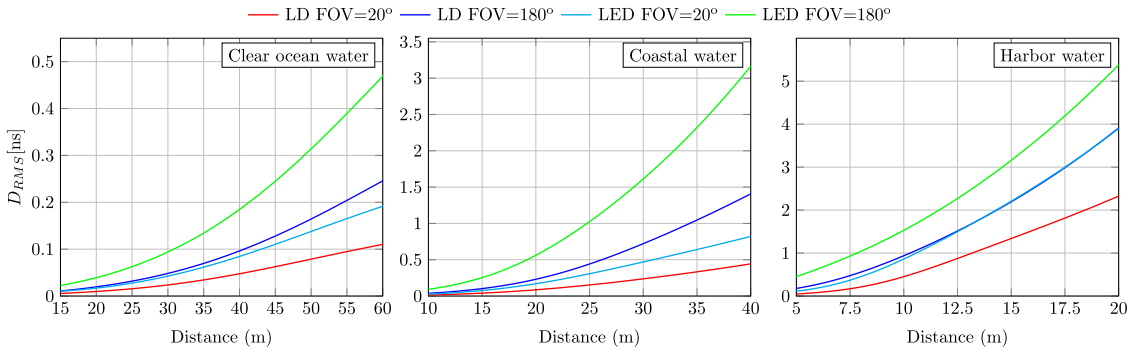

Fig. 4. RMS delay spread, $D_{\text{RMS}}(d)$, as a function of distance for clear ocean, coastal and harbor waters when a receiver aperture diameter of $D = 50$ cm and different transmitter sources are considered for different values of the receiver FOV.

sophisticated communication techniques in order to reduce such a dispersive effect and extend the coverage area.

Finally, the analytical results obtained via Eq. (11) with no scattering ($F_c = 1$) are also depicted with dash dot lines in order to corroborate that the Beer Lambert's law underestimates the dispersive component that allows to recollect more photons, specially those that are reflected multiple times until reaching the receiver. This fact is better reflected in turbid environments than in clear ocean water due to the fact that scattering is more significant.

4.3 RMS Delay Spread Analysis

In order to quantify the impact of the temporal dispersion produced by the UOWC channel, we compute analytically the channel RMS delay spread D_{RMS} as a function of distance. This indicator results in being very useful since it provides some valuable information with regard to the maximum achievable data rate without requiring channel equalization systems and methods [30], [31]. Therefore, from the expression obtained for the CIR in Eq. (6), we can find an analytical expression to quantify such an indicator as follows

$$D_{\text{RMS}} = k \cdot \sqrt{\frac{\int_0^\infty (t-\mu)^2 h_{\text{BP}}^2(t)dt}{\int_0^\infty h_{\text{BP}}^2(t)dt}} = k \cdot \sqrt{\frac{1}{\beta_2}\left(\frac{\beta_1(1-2\beta_1)}{1-2\beta_2} + (1-2\beta_1)\mu + \beta_2\mu^2\right)}, \tag{19}$$

where the mean delay μ can be readily derived as

$$\mu = \frac{\int_0^\infty t h_{\text{BP}}^2(t)dt}{\int_0^\infty h_{\text{BP}}^2(t)dt} = \frac{\beta_1(1-2\beta_1)}{\beta_2(1-2\beta_2)}. \tag{20}$$

Substituting Eq. (20) into Eq. (19), and after performing some algebraic manipulations, we can write the RMS delay spread as a function of distance as follows

$$D_{\text{RMS}}(d) = \frac{k(d)}{2}\sqrt{\frac{(2\beta_1(d)-1)\,(2\beta_1(d)+2\beta_2(d)-1)}{\beta_2(d)^2\,(2\beta_2(d)-1)}} \quad [ns]. \tag{21}$$

Next, we depict the RMS delay spread D_{RMS} as a function of distance in Fig. 4. As expected, such an indicator is highly dependent on the type of water, transmitter source, link distance and receiver FOV. We can see that as scattering process becomes more severe, the RMS delay spread increases quickly regardless of the major UOWC system parameters. Hence, there is more risk of ISI in coastal and harbor waters than in clear ocean water. But the most striking thing is that the impact of the receiver FOV on the RMS delay spread, since larger values of the RMS delay spread are obtained for larger receiver FOVs. We can clearly conclude that larger receiver FOVs are able

to recollect more emitted photons, as proved in [1], but at the same time the RMS delay spread will be larger. However, smaller receiver FOVs recollect less emitted photons and, hence, the RMS delay spread will be smaller. This is directly related to the performance of UOWC systems, since smaller values of the RMS delay spread will enable higher data rates. Similar conclusions were drawn for indoor visible light communication channels [32]. Therefore, there exits a compromise in terms of UOWC system design between increasing the receiver FOV to maximize the received intensity, which is needed in harbor waters, or decreasing the receiver FOV, which is feasible in clear ocean water, to increase the data rate. Obviously, equalization techniques can be used to increase the data rate at the expense of increasing the receiver complexity.

Temporal dispersion is directly related to the bandwidth of the UOWC system, where the maximum data rate should be below $1/10D_{\mathrm{RMS}}$, i.e., $R_{\mathrm{MAX}} \leq 1/10D_{\mathrm{RMS}}$ to avoid ISI. In other words, if the RMS delay spread of an underwater channel is small relative to the pulse duration, the ISI may be neglected. For instance, if we consider an UOWC link distance of 20 m and an LD, we obtain values of the maximum data rates of $R_{\mathrm{MAX}} = \{5.263, 0.43, 0.025\}$ Gbps for clear ocean, coastal and harbor waters, respectively, when a receiver FOV of 180° is used. Analogously, if we now consider an UOWC link distance of 20 m and an LED, we obtain values of the maximum data rates of $R_{\mathrm{MAX}} = \{2.564, 0.178, 0.018\}$ Gbps for clear ocean, coastal and harbor waters, respectively, when a receiver FOV of 180° is used. On the one hand, it is confirmed once again that turbidity of the water is a limiting factor to get long and reliable underwater communication links, as well as high data rates. Moreover, we observe a remarkable data rate reduction between clear ocean and turbid waters for the same distance. For a link distance of 20 m and using an LD, there is a data rate reduction of 91.8% between clear ocean and coastal waters, and 99.5% between clear ocean and harbor waters. When an LED is used, there is a data rate reduction of 93% between clear ocean and coastal waters, and 99.3% between clear ocean and harbor waters. On the other hand, it is also confirmed that higher data rates are achieved when an LD is used in comparison with an LED at the transmitter-side. Data rate increases of 51.3%, 58.6%, and 28% are achieved when using LD instead of LED for an UOWC link distance of 20 m in clear ocean, coastal and harbor waters, respectively.

5. Conclusion

A novel and unified channel modeling for UOWC systems based on the mixture of two Gamma functions by using two degrees of freedom and taking into account channel path loss has been thoroughly analyzed and verified by photon-tracing-based Monte-Carlo simulations in this paper.

On the one hand, we have been able to express the CIR of UOWC systems not only as a function of time, but also as a function of distance, obtaining a high degree of precision measured by the coefficient of determination R^2, always above 0.97 under different scattering conditions. We have also developed an expression to compute channel path loss as a function of distance, which is valid for different transmitter sources. Additionally, thanks to having expressed the CIR as a superposition of one impulsive component and one dispersive component, we have been able to determine at which distance the underwater channel behaves as an impulsive one or as a non-impulsive one. In terms of high-speed systems design, these outcomes are really interesting and valuable. On the other hand, by exploiting the proposed CIR, we have observed that the receiver FOV presents an interesting impact on key indicators such as the RMS delay spread. In other words, the maximum data rate allowed to avoid ISI depends also on the receiver FOV. To the best of our knowledge, these conclusions have not been drawn in any early paper. These results are of great importance for the optics community since they can be directly applied to UOWC performance analysis.

In the future, we plan to link the predicted CIR with the rest of UOWC channel parameters, as well as mitigate the effect of ISI produced by strong scattering even when oceanic turbulence and pointing errors take place. Additionally, further efforts should be also dedicated to studying key performance indicators such as bit error rate, as well as the maximum channel capacity that UOWC systems can achieve under different scattering conditions.

References

[1] R. Boluda-Ruiz, P. Rico-Pinazo, B. Castillo-Vazquez, A. Garcia-Zambrana, and K. Qaraqe, "Time-dispersion and signal attenuation analysis of underwater optical wireless communication links," in *Proc. IEEE Global Commun. Conf.*, 2019, pp. 1–6.

[2] "Worldatlas: How much of the ocean is still unexplored?" 2018. [Online]. Available: https://www.worldatlas.com/articles/how-much-of-the-ocean-is-still-unexplored.html

[3] S. Dang, O. Amin, B. Shihada, and M.-S. Alouini, "What should 6G be?" *Nature Electron.*, vol. 3, no. 1, pp. 20–29, 2020.

[4] "The sonardyne site: Bluecomm underwater optical communications. Sonardyne International Ltd." 2020. [Online]. Available: http://www.sonardyne.com/

[5] H. Kaushal and G. Kaddoum, "Underwater optical wireless communication," *IEEE Access*, vol. 4, pp. 1518–1547, 2016.

[6] Z. Zeng, S. Fu, H. Zhang, Y. Dong, and J. Cheng, "A survey of underwater optical wireless communications," *IEEE Commun. Surv. Tut.*, vol. 19, no. 1, pp. 204–238, Jan.–Mar. 2017.

[7] X. Sun *et al.*, "A review on practical considerations and solutions in underwater wireless optical communication," *IEEE/OSA J. of Lightw. Technol.*, vol. 38, no. 2, pp. 421–431, Jan. 2020.

[8] A. Jurado-Navas, N. G. Serrato, J. Garrido-Balsells, and M. Castillo-Vázquez, "Error probability analysis of OOK and variable weight MPPM coding schemes for underwater optical communication systems affected by salinity turbulence," *OSA Continuum*, vol. 1, no. 4, pp. 1131–1143, 2018.

[9] C. D. Mobley *Light and Water: Radiative Transfer in Natural Waters*. New York, NY, USA: Academic, 1994.

[10] S. Tang, Y. Dong, and X. Zhang, "Impulse response modeling for underwater wireless optical communication links," *IEEE Trans. on Commun.*, vol. 62, no. 1, pp. 226–234, Jan. 2014.

[11] H. Zhang and Y. Dong, "Impulse response modeling for general underwater wireless optical MIMO links," *IEEE Commun. Mag.*, vol. 54, no. 2, pp. 56–61, Feb. 2016.

[12] M. V. Jamali, P. Nabavi, and J. A. Salehi, "MIMO underwater visible light communications: Comprehensive channel study, performance analysis, and multiple-symbol detection," *IEEE Trans. on Veh. Technol.*, vol. 67, no. 9, pp. 8223–8237, Sep. 2016.

[13] Y. Li, M. S. Leeson, and X. Li, "Impulse response modeling for underwater optical wireless channels," *Appl. Opt.*, vol. 57, no. 17, pp. 4815–4823, Jun. 2018.

[14] M. Elamassie, F. Miramirkhani, and M. Uysal, "Performance characterization of underwater visible light communication," *IEEE Trans. Commun.*, vol. 67, no. 1, pp. 543–552, Jan. 2019.

[15] R. Yuan, J. Ma, P. Su, Y. Dong, and J. Cheng, "Monte-Carlo integration models for multiple scattering based optical wireless communication," *IEEE Trans. Commun.*, vol. 68, no. 1, pp. 334–348, Jan. 2020.

[16] V. I. Haltrin, "Chlorophyll-based model of seawater optical properties," *Appl. Opt.*, vol. 38, no. 33, pp. 6826–6832, 1999.

[17] C. Gabriel, M.-A. Khalighi, S. Bourennane, P. Léon, and V. Rigaud, "Monte-Carlo-based channel characterization for underwater optical communication systems," *IEEE/OSA J. of Opt. Commun. and Netw.*, vol. 5, no. 1, pp. 1–12, Jan. 2013.

[18] L. G. Henyey and J. L. Greenstein, "Diffuse radiation in the galaxy," *Astrophysical J.*, vol. 93, pp. 70–83, 1941.

[19] C. T. Geldard, J. Thompson, and W. O. Popoola, "An overview of underwater optical wireless channel modelling techniques," in *Proc. Int. Symp. Electron. Smart Devices*, 2019, pp. 1–4.

[20] H. Ding, G. Chen, A. K. Majumdar, B. M. Sadler, and Z. Xu, "Modeling of non-line-of-sight ultraviolet scattering channels for communication," *IEEE J. on Sel. Areas Commun.*, vol. 27, no. 9, pp. 1535–1544, Dec. 2009.

[21] A. García-Zambrana, R. Boluda-Ruiz, C. Castillo-Vázquez, and B. Castillo-Vázquez, "Novel space-time trellis codes for free-space optical communications using transmit laser selection," *Opt. Express*, vol. 23, no. 19, pp. 24 195–24 211, Sep. 2015.

[22] R. Boluda-Ruiz, A. García-Zambrana, B. Castillo-Vázquez, C. Castillo-Vázquez, and K. Qaraqe, "On the beam width optimization for the ergodic capacity of FSO channels with misalignment errors modeled by beckmann distributions," *IEEE Photon. J.*, vol. 10, no. 5, 2018, Art. no. 7907414.

[23] F. Hanson and M. Lasher, "Effects of underwater turbulence on laser beam propagation and coupling into single-mode optical fiber," *Appl. Opt.*, vol. 49, no. 16, pp. 3224–3230, 2010.

[24] I. S. Gradshteyn and I. M. Ryzhik, *Table of integrals, series and products*, 7th ed., New York, NY, USA: Academic, 2007.

[25] S. D. Dubey, "Compound gamma, beta and f distributions," *Metrika*, vol. 16, no. 1, pp. 27–31, 1970.

[26] L. C. Andrews and R. L. Phillips, *Laser beam propagation through random media*, vol. 1. Bellingham, WA, USA: SPIE, 2005.

[27] S. Arnon, "Underwater optical wireless communication network," *Opt. Eng.*, vol. 49, no. 1, 2010, Art. no. 015001.

[28] B. M. Cochenour, L. J. Mullen, and A. E. Laux, "Characterization of the beam-spread function for underwater wireless optical communications links," *IEEE J. Ocean. Eng.*, vol. 33, no. 4, pp. 513–521, Oct. 2008.

[29] L. Mullen, D. Alley, and B. Cochenour, "Investigation of the effect of scattering agent and scattering albedo on modulated light propagation in water," *Appl. Opt.*, vol. 50, no. 10, pp. 1396–1404, 2011.

[30] J. M. Kahn and J. R. Barry, "Wireless infrared communications," in *Proc. IEEE*, vol. 85, no. 2, pp. 265–298, Feb. 1997.

[31] A. Goldsmith, *Wireless Communications*. Cambridge, U.K.: Cambridge Univ. Press, 2005.

[32] M. Kavehrad, M. S. Chowdhury, and Z. Zhou, *Short-Range Optical Wireless: Theory and Applications*, Hoboken, NJ, USA: Wiley, 2016.